Journal of Nuclear Medicine, published on July 9, 2020 as doi:10.2967/jnumed.120.245068

Effect of tumor perfusion and receptor density on tumor control probability in ^{177}Lu-DOTATATE therapy: An *in silico* analysis for standard and optimized treatment

Luis David Jiménez-Franco[1], Gerhard Glatting[2,3], Vikas Prasad[2], Wolfgang A. Weber[4], Ambros J. Beer[2], Peter Kletting[2,3]

[1]*ABX-CRO advanced pharmaceutical services Forschungsgesellschaft mbH, Dresden, Germany*

[2]*Department of Nuclear Medicine, Ulm University, Ulm, Germany*

[3]*Medical Radiation Physics, Department of Nuclear Medicine, Ulm University, Ulm, Germany*

[4]*Department of Nuclear Medicine, Klinikum Rechts der Isar,* Technische Universität München*, Munich, Germany*

First author: Dr. Luis David Jimenez Franco
ABX-CRO
D - 01307 Dresden, Germany
Telephone number: +49 173 197 1898
E-mail address: luisdavid.jimenez@abx-cro.com

Corresponding author:
Dr. Peter Kletting
Department of Nuclear Medicine, Ulm University
D - 89081 Ulm, Germany
Tel./(Fax): ++49 731 500 61371/(61302)
e-mail: peter.kletting@uniklinik-ulm.de

Word count of text: 4981

Running title: Tumor perfusion and receptor density

ABSTRACT

The aim of this work was to determine a minimal tumor perfusion and receptor density for ^{177}Lu-DOTATATE therapy using physiologically based pharmacokinetic (PBPK) modeling considering 1) a desired tumor control probability (TCP) of 99% and 2) a maximal tolerated biologically effective dose (BED_{max}) for organs at risk (OARs) in the treatment of neuroendocrine tumors and meningioma. **Methods**: A recently developed PBPK model was employed. Nine virtual patients (i.e. individualized PBPK models) were used to perform simulations of pharmacokinetics for different combinations of perfusion (0.001-0.1 mL/g/min) and receptor density (1-100 nmol/L). The TCP for each combination was determined for three different treatment strategies: 1) for a standard treatment (4 cycles of 7.4 GBq and 105 nmol), 2) maximizing the number of cycles based on BED_{max} for red marrow and kidneys and 3) for 4 cycles with optimized ligand amount and activity. The red marrow and the kidneys (BED_{max} of 2 Gy_{15} and 40 $Gy_{2.5,}$ respectively) were assumed to be OARs. Additionally, the influence of varying glomerular filtration rates, kidney somatostatin receptor densities, tumor volumes and release rates was investigated. **Results**: To achieve a TCP ≥99% in the standard treatment, a minimal tumor perfusion of 0.036±0.023 mL/g/min and receptor density of 34±20 nmol/L were determined for the nine virtual patients. With the optimization of the number of cycles, the minimum values of perfusion and receptor density were considerably lower with 0.022±0.012 mL/g/min and 21±11 nmol/L, respectively. However, even better results (perfusion = 0.018±0.009 mL/g/min and receptor density = 18±10 nmol/L) were obtained for strategy 3. The release rate of

^{177}Lu (or labelled metabolites) from tumor cells had the strongest effect on the minimal perfusion and receptor density for standard and optimized treatments. **Conclusion**: PBPK modeling and simulations represent an elegant approach to individually determine the minimal tumor perfusion and minimal receptor density required to achieve an adequate TCP. This computational method can be employed in the radiopharmaceutical development process for ligand and target selection for specific types of tumors. In addition, this method could be used to optimize clinical trials.

Keywords: Minimal tumor perfusion, minimal receptor density, PBPK modeling, tumor control probability, ^{177}Lu-DOTATATE

INTRODUCTION

Tumor uptake of radioligands is determined by their affinity for their respective targets, the expression level of the target as well as the perfusion. In molecular radiotherapy, perfusion can become a limiting factor for tumor uptake and absorbed dose when using ligands with small molecular size which are rapidly cleared from the circulation by the kidneys (*1,2*). Due to the recent clinical success of molecular radiotherapy for neuroendocrine tumors (NETs) and prostate cancer, there is an enormous interest in identifying novel targets and radioligands to expand the use of molecular radiotherapy to other malignancies (*3,4*). The selection of promising targets and ligands for further testing is currently performed by qualitative ("semi-quantitative") assessment of the target expression as well as with in-vitro studies of the ligand affinity. In-vivo tumor uptake is then usually assessed in tumor bearing mice. However, these animal studies may be misleading due to marked differences between mouse and human cardiovascular physiology resulting in different blood clearance rates as well as differences in perfusion between human tumors and subcutaneous xenografts (*5*). In addition, target expression may differ significantly between xenografts and human tumors. Therefore, a quantitative model to predict radioligand uptake in tumors based on target expression levels and perfusion would be of great value for radioligand development and for the optimization of the assessment process. Such a model could, for example, estimate the minimal tumor perfusion and target expression levels required to achieve a certain tumor control probability (TCP) while considering the maximum tolerated biologically effective doses (BED_{max}) for normal tissues.

To our knowledge, no systematic, quantitative analysis of the impact of receptor density and perfusion on tumor uptake of radioligands has been conducted. Furthermore, it has not been analyzed to which extent low BED due to poor perfusion can be overcome by individualized treatment, e.g. adjusting the injected activity and ligand amount or the number of treatment cycles (*6,7*). Whole body physiologically based pharmacokinetic (PBPK) modeling allows addressing these questions (*8-11*). With known ranges of perfusions and receptor densities in tumor and other physiological parameters for normal tissues, simulations can 1) determine the feasibility of using that target structure for therapy, and 2) optimize the administered ligand amount and activity.

In this study, we performed this analysis for the treatment of NETs and meningioma with ^{177}Lu-DOTATATE, a peptide with high affinity to the somatostatin receptor type 2 (SSTR2) (*6,7*). Specifically, we determined the minimal tumor perfusion and receptor density based on PBPK modeling considering 1) a desired TCP of 99% and 2) the BED_{max} for organs at risk (OARs). The TCP was calculated for various combinations of tumor perfusion (0.001 - 0.1 mL/g/min) and receptor density (1-100 nmol/L) in nine virtual patients (i.e. individualized PBPK models) with NETs (n = 5) or meningioma (n = 4). Kidneys (BED_{max} of 40 $Gy_{2.5}$) and red marrow (BED_{max} of 2 Gy_{15}) were considered to be OARs. One tumor lesion per virtual patient was investigated. The TCP was calculated for each virtual patient and combination of tumor perfusion and receptor density for standard and optimized therapy. Additionally, we determined the influence of the glomerular filtration rate (GFR), kidney SSTR2

density, release rate of ^{177}Lu/radiolabeled metabolites from tumor cell and tumor volume.

METHODS

PBPK Model

The development of the PBPK model and the estimation of the individual model parameters of the virtual patients are described elsewhere (*6,7*) and in the supplemental material (supplemental A, Tables 1-3). In brief, all major physiological and physical mechanisms, i.e. distribution via blood flow, binding to serum proteins, extravasation, non-linear SSTR2 specific binding, internalization, degradation and release, excretion and physical decay are included in the model (supplemental A, Figures 1-3). Kidney uptake is assumed to be predominantly SSTR2-specific due to the high kidney SSTR2 expression, the high affinity of ^{177}Lu-DOTATATE to the SSTR2 and the administration of amino acids, which substantially decreases the non-specific uptake. One tumor lesion per virtual patient was considered. The model was implemented in Matlab/Simulink® R2017a (MathWorks, Natick, MA, USA).

Virtual Patients

In this work, a virtual patient is defined as a PBPK model with a set of parameters determined by fitting the model to individual time activity data and directly measured quantities. The model and individual model parameters were taken from Jimenez et al. (*7*). Nine virtual patients were investigated, which differ regarding GFR, SSTR2 expression in normal tissue, tumor volume, release rates from tumor and normal tissue and other individualized parameters (supplemental A, Tables 2 and 3).

No changes in tumor perfusion and receptor expression between the cycles were assumed as well as no tumor growth or shrinkage was considered.

Absorbed Dose, Biologically Effective Dose and Tumor Control Probability

The PBPK model structure was combined with a radiobiological model for BED and TCP calculations (supplemental B). Absorbed doses, BEDs and TCP values were calculated as described by Jimenez et al. (*7*) (supplement B). In short, absorbed doses considering only self-irradiation were calculated for the kidneys while for the red marrow both self- and cross-irradiation were considered (supplemental B, Table 1). Tumor absorbed doses were calculated using a sphere model (*12*) (supplemental B, Table 2).

For the BED calculations, α/β ratios (the parameters of the linear-quadratic model of cell survival) of 2.5 Gy, 15 Gy and 10 Gy were assumed for the kidneys, red marrow and tumor lesions, respectively (*7*) (supplemental B). The cell repair rates used for the BED calculations were $\ln(2)/2.8\ h^{-1}$ for the kidneys, $\ln(2)/1.0\ h^{-1}$ for the red marrow and $\ln(2)/1.5\ h^{-1}$ for the tumor lesions (*13*).

TCP values were determined assuming that the cell survival fraction was equal for all the cycles and that there were no physiological or radiobiological changes in the organ and tumor parameters throughout the cycles. Thus, Eq. (1) was used for the TCP calculations for multiple cycles as follows (*7*) (supplemental B):

$$TCP = e^{-n_0 \cdot \left(SF_c{}^{Nc}\right)} \qquad (1)$$

where n_0 is the initial number of tumor clonogenic cells, SF_c is the tumor survival fraction for the first dose cycle and Nc is the number of cycles. The number of clonogenic cells for each lesion was determined considering its mass and a clonogenic cell density of 1.12×10^5 cells/g (*14*). Survival fractions were calculated from the BED values assuming a radiosensitivity value α of 0.35 Gy^{-1} for all tumor lesions (*14*).

Simulations with Individual Virtual Patients

The TCP values were calculated for different combinations of tumor receptor density (i.e. number of receptors per mass $[R]_{tu}$) and perfusion (i.e. blood flow per mass f_{tu}). All other parameters of the virtual patients were unchanged. The tumor perfusion and receptor density were varied from 0.001 to 0.1 mL/g/min (steps of 0.001 mL/g/min) and from 1 to 100 nmol/L (steps of 1 nmol/L), respectively. The choices of the maximal investigated tumor receptor density and perfusion values were based on the literature (*6,15*).

Different Treatment Strategies

The TCP was investigated for all combinations of tumor receptor density and perfusion for standard ^{177}Lu-DOTATATE therapy (4 cycles of 7.4 GBq and 105 nmol) (*16*) (strategy 1) and for individualized therapy based on dosimetry results (strategy 2) and on the estimated optimal ligand amount and activity (strategy 3) (Table 1). For strategies 1 and 2, a ligand amount of 105 nmol (~150 µg) is used to represent the standard therapy, as the consensual ligand amount is between 100 µg (~70 nmol) and 200 µg (~139 nmol) (*16*). For strategies 2 and 3, the kidneys and the red marrow were

assumed to be the OARs with BED_{max} of 40 $Gy_{2.5}$ and 2 Gy_{15}, respectively(*7*). For strategy 3, the highest TCP without exceeding BED_{max} for the kidneys and the red marrow (*7*) was determined by simulations with different ligand amounts (25, 50, 75, 100, 125, 150, 175, 200, 250, 350 and 500 nmol) and pertaining maximal activities (*7*).

Additionally, the actual dose-limiting organ (kidneys or red marrow) was identified for each combination of tumor perfusion and receptor density for all virtual patients.

Simulations with Population Median Virtual Patient

To analyze the influence of other important parameters on the minimal tumor receptor density and perfusion, simulations with two tumor-specific and two normal-tissue-specific parameters were conducted for all strategies for a population virtual patient with median parameters from the nine virtual patients: The effects of varying the tumor volume (0.1, 1, 10 and100 mL), the release rate from the tumor (10^{-3}, 10^{-4}, 10^{-5} and 10^{-6} min^{-1}) (*17*), GFR (30, 60, 90 and 120 $mL \cdot min^{-1}$) and SSTR2 expression in the kidneys (2.5, 5, 7.5 and 10 $nmol \cdot mL^{-1}$) (*6,7*) were investigated. These parameters were selected as they vary considerably between the virtual patients: tumor volume (2-2520 mL), release rate from the tumor ($0\text{-}3 \cdot 10^{-4}$ min^{-1}), GFR (28-133 mL/min) and SSTR2 density in the kidneys (2.3-8.8 nmol/L).

Definition of the Minimal Tumor Perfusion and Receptor Density

As there is no unique combination of tumor perfusion and receptor density leading to TCP ≥99% and to ease the comparison for the different simulations, the

combination with the smallest standardized Euclidean distance (standardized by range) to the origin (0 nmol/L, 0 mL/g/min) was selected to represent the minimum tumor perfusion and receptor density.

RESULTS

Minimal Tumor Perfusion and Receptor Density

Figure 1 shows the simulation results for all combinations of tumor perfusion and receptor density averaged over the virtual patients for the studied strategies. For a standard treatment schedule of ^{177}Lu-DOTATATE, a minimum SSTR2 density of 55 nmol/l and a minimum perfusion of 0.062 mL/g/min is necessary for a TCP ≥99% (Figure 1A). For strategy 2, the minimum tumor perfusion and SSTR2 density are 0.031 mL/g/min and 31 nmol/l, respectively (Figure 1B). For strategy 3, the minimum values are 0.026 mL/g/min and 27 nmol/l, respectively (Figure 1C). For a receptor density < 25 nmol/l, a TCP ≥99% could not be achieved for any of the evaluated perfusion values and strategies. The minimal tumor perfusion and receptor density were considerably lower on average for strategy 2 compared to strategy 1 (Figure 1B compared to 1A). A further improvement was observed for strategy 3 (Figure 1D). Table 2 presents one combination (defined by the smallest standardized Euclidian distance) of the minimal tumor perfusion and receptor density for each strategy and each virtual patient to achieve a TCP ≥99%.

Dose-limiting Organs

The defined BED limits for the OARs were not exceeded for any of the nine virtual patients with strategy 1. For strategy 2, the BED_{max} for the kidneys (n = 6) or red marrow (n = 3) was reached after 4 to 9 cycles (median = 6). Figure 2 shows the fraction among all virtual patients in which the kidneys were the dose-limiting organ

for strategy 3. For the remaining virtual patients, the red marrow was dose-limiting (Figure 2 subtracted from 100%). For strategy 3, the likelihood that the kidneys are the dose-limiting organ increases with increasing tumor perfusion and decreasing receptor density (Figure 2) as lower ligand amounts are required for optimal TCP (Figure 3A). On the other hand, for strategy 3, the higher the receptor density and the lower the perfusion, the more likely is the red marrow dose-limiting (Figure 2) due to increasing optimal ligand amounts (Figure 3A).

Optimal Amounts and Activities

Figure 3 depicts the optimal peptide amount (Figure 3A) and activity (Figure 3B) for all combinations averaged over all virtual patients. A red line encompassing the consensual peptide amount range (70 nmol to 139 nmol) is shown in Figure 3A (*16*). The average optimal activity was higher than the suggested maximum activity (7.4 GBq) for all the explored combinations (Figure 3B) (*16*). Figure 3A shows that for higher perfusion (> 0.059 mL/g/min) and lower receptor density (< 11 nmol/L) the optimal peptide amount is lower than the minimal consensual ligand amount (70 nmol). Similarly, for low tumor perfusion (< 0.027 ml/g/min) and high receptor density (> 60 nmol/L), the optimal amount is higher than the maximal consensual ligand amount (139 nmol). However, the optimal amounts are within the consensus range for most of the investigated combinations of tumor perfusion and receptor density.

Simulations with Population Median Virtual Patient

The results for the simulations with the population median virtual patient are presented in Table 3. The tumor release rate is the most sensitive parameter in all strategies. The effect of changes in the GFR is stronger for strategy 1, where for higher GFR values, higher tumor perfusions and receptor densities are required to achieve TCP ≥99%. The influence of variations in the GFR is considerably reduced by optimizing cycles and/or ligand amount and activity. Variations in the tumor volume produce a relatively small variation in the minimum tumor perfusion and receptor density for all the evaluated strategies (Table 3).

DISCUSSION

PBPK modeling is increasingly used in the development of drugs and for therapy optimization (*18*). Here we employed a mathematical model combining a PBPK structure with BED and TCP calculations (*6,7*) to investigate the effect of the tumor perfusion and SSTR2 receptor density on the effectiveness of ^{177}Lu-DOTATATE therapy in patients with NETs and meningioma.

Our results indicate that for a standard treatment a minimum SSTR2 density of 55 nmol/l and a minimum perfusion of 0.062 mL/g/min are necessary for a TCP ≥99% (Figure 1A). As this combination is presented for the standardized Euclidian distance to the origin, receptor densities > 55 nmol/l may allow for TCP ≥99%, even at lower tumor perfusions (Figure 1). Conversely, higher perfusion values could to some extent compensate for a lower receptor density. Nevertheless, our simulations indicate that well-defined limits exist for both tumor receptor density and perfusion that determine the effectiveness of the ^{177}Lu-DOTATATE therapy.

A second important finding of our study is that individualized treatment strategies considering BED_{max} for the red marrow and the kidneys can substantially reduce the limitations for tumor perfusion and receptor density (Figure 1B-1D). By adjusting the peptide amount and injected activity, a TCP ≥99% was achieved for a 2-fold lower receptor density and a 2.4-fold lower tumor perfusion compared to standard treatment (Figure 1).

These findings have several implications for ^{177}Lu-DOTATATE therapy. First of all, it is ensuring that for standard and optimized ^{177}Lu-DOTATATE therapy, the

calculated individual minimal perfusions (~0.004-0.07 mL/g/min) are well below the average tumor perfusion of NET primaries(*19*), NET metastases(*20*) or meningiomas (*21*) (all > 0.1 mL/g/min). Thus, tumor perfusion does not appear to be a limiting factor for ^{177}Lu-DOTATATE therapy for these diseases. However, the tumor SSTR2 expression found in these virtual patients (determined by fitting to time activity data in Kletting et al.[5]) is about 1.9-fold lower on average than the herein identified minimal receptor density for standard therapy, 1.2-fold lower for optimized cycles and similar for optimized ligand amount and activity (Table 2). Thus, effectiveness can potentially be improved by ligands with higher SSTR2 density and/or longer tumor retention such as some SSTR2 antagonists that have recently entered clinical testing (*22*).

Second, our results strongly argue for performing dosimetry to improve the success of ^{177}Lu-DOTATATE therapy. Peri-therapeutic measurements and absorbed dose calculation help in deciding on whether to increase the number of cycles compared to the standard treatment (median optimal number of cycles = 6). A further improvement would be treatment planning, where ligand amount and activity are individualized prior to the first cycle. Incorporating PET/MR or PET/CT measurements in combination with additional prior knowledge (e.g. GFR measurements) and PBPK modeling might allow to individually estimate perfusion and receptor density of the clinically most relevant lesions prior to therapy. Thus, tailoring therapy might increase the TCP for many NETs and meningioma substantially. However, to fully incorporate such approaches into clinical decision making, these models need to be refined regarding tumor changes after each cycles (*8*).

The application of this PBPK model goes beyond optimizing ^{177}Lu-DOTATATE treatment of NETs and meningioma as SSTR2 is expressed by a variety of other malignancies such as non-Hodgkin lymphomas, renal cell cancer and others (*3,4*). Thus, PBPK modeling can be used to assess if molecular radiotherapy with ^{177}Lu-DOTATATE or with other SSTR2 ligands are potentially effective therapies for these tumor types or if the perfusion and/or the SSTR2 expression are too low to achieve the expected therapeutic effect. Furthermore, PBPK modeling and the proposed method can also be applied for novel targets as soon as the typical ranges for the number of binding sites and for the perfusion of the targeted tumor type are known.

In general, the complexity of PBPK models (*23*) depends on the knowledge of the biological systems and the scientific question to be answered. To demonstrate the relationship of perfusion, receptor density, activity and ligand amount, in scenario 3 we optimized the TCP for only one tumor lesion. Consequently, intra-individual variability of the tumor characteristics was not considered, which could have influenced the TCP calculations. For treatment planning, more lesions could be taken into account as described by Jimenez et al. (*7*). For the actual treatment planning, including temporal and spatial changes of the tumor SSTR2 expression, perfusion and radiosensitivity might improve the predictions. Heterogeneity of the target expression, the perfusion and radiosensitivities at the microscopic level may lead to an inhomogeneous absorbed dose distribution. It is currently unknown how this heterogeneity will affect the TCP in molecular radiotherapy, and the effect may vary for different radionuclides. However, in principle, this heterogeneity could be included in the model once data on

the microscopic heterogeneity of the SSTR2 expression, perfusion and radiosensitivity become available.

CONCLUSION

A method was developed based on PBPK and radiobiological modeling to identify a minimal tumor perfusion and receptor density which allows a defined (here ≥99%) tumor control probability after ^{177}Lu-DOTATATE therapy. The algorithm takes into account previously determined expression levels in normal tissues and BED limits for the kidneys and the red marrow. The method can be easily adapted to other tumors/ligands and might be helpful in the development and validation of new ligands and in the optimization of clinical trials.

DISCLOSURE

The authors declare that they have no competing interests.

ACKNOWLEDGEMENTS

The authors gratefully acknowledge grants by the “Deutsche Forschungsgemeinschaft” (German Research Foundation, KL2742/2-1, BE4393/1-1, GL236/11-1, SFB824 Project B11, SFB1279 Project Z02).

KEY POINTS

QUESTION: What is the minimal tumor perfusion and receptor density for a successful treatment using a specific target (here SSTR2) and ligand in ^{177}Lu- DOTATATE therapy?

PERTINENT FINDINGS: The minimal flow and receptor density for achieving a tumor control probability ≥99% for a standard therapy were 0.036±0.023 mL/g/min and 34±20 nmol/L. These parameter values were determined for nine virtual patients using PBPK and radiobiological modeling. Individually optimizing the number of cycles or the ligand and activity amount allows even considerably lower perfusion and receptor densities.

IMPLICATIONS FOR PATIENT CARE: Individually optimized therapy with ^{177}Lu-DOTATATE with respect to the number of cycles and/or the amounts of ligand and activity may considerably improve therapy.

REFERENCES

1. Thurber GM, Weissleder R. A systems approach for tumor pharmacokinetics. *PLoS ONE.* 2011;6:e24696.

2. Thurber GM, Weissleder R. Quantitating antibody uptake in vivo: conditional dependence on antigen expression levels. *Mol Imaging Biol.* 2010;13: 623-32

3. Haberkorn U, Mier W, Kopka K, Herold-Mende C, Altmann A, Babich J. Identification of ligands and translation to clinical applications. *J Nucl Med.* 2017;58:27s-33s.

4. Reubi JC, Waser B, Mäcke H, Rivier J. Highly Increased ^{125}I-JR11 Antagonist Binding In Vitro Reveals Novel Indications for sst2 Targeting in Human Cancers. *J Nucl Med.* 2017;58:300-306.

5. White CR, Kearney MR. Metabolic Scaling in Animals: Methods, Empirical Results, and Theoretical Explanations. *Comprehensive Physiology.* 2014;4:231-256.

6. Kletting P, Kull T, Maaß C, et al. Optimized peptide amount and activity for ^{90}Y-Labeled DOTATATE therapy. *J Nucl Med.* 2016;57:503-508.

7. Jiménez-Franco LD, Kletting P, Beer AJ, Glatting G. Treatment planning algorithm for peptide receptor radionuclide therapy considering multiple tumor lesions and organs at risk. *Med Phys.* 2018;45:3516-3523.

8. Kletting P, Thieme A, Eberhardt N, et al. Modeling and predicting tumor response in radioligand therapy. *J Nucl Med.* 2019;60:65-70.

9. Begum NJ, Thieme A, Eberhardt N, et al. The effect of total tumor volume on the biologically effective dose of tumor and kidneys for ^{177}Lu-labelled PSMA peptides. *J Nucl Med.* 2018;6:929-933.

10. Kletting P, Schuchardt C, Kulkarni HR, et al. Investigating the Effect of Ligand Amount and Injected Therapeutic Activity: A Simulation Study for ^{177}Lu-Labeled PSMA-Targeting Peptides. *PLoS ONE.* 2016;11:e0162303.

11. Thiel C, Smit I, Baier V, et al. Using quantitative systems pharmacology to evaluate the drug efficacy of COX-2 and 5-LOX inhibitors in therapeutic situations. *NPJ Syst Biol Appl.* 2018;4:28.

12. Stabin MG, Siegel JA. Physical models and dose factors for use in internal dose assessment. *Health Phys.* 2003;85:294-310.

13. Cremonesi M, Botta F, Di Dia A, et al. Dosimetry for treatment with radiolabelled somatostatin analogues. A review. *Q J Nucl Med Mol Imaging.* 2010;54:37-51.

14. Fowler JF. 21 years of biologically effective dose. *Br J Radiol.* 2010;83:554-568.

15. Vaupel P, Kallinowski F, Okunieff P. Blood flow, oxygen and nutrient supply, and metabolic microenvironment of human tumors: a review. *Cancer Res.* 1989;49:6449-6465.

16. Zaknun J, Bodei L, Mueller-Brand J, et al. The joint IAEA, EANM, and SNMMI practical guidance on peptide receptor radionuclide therapy (PRRNT) in neuroendocrine tumours. *Eur J Nucl Med Mol Imaging.* 2013,40:1-17.

17. Fung EK, Cheal SM, Fareedy SB, et al. Targeting of radiolabeled J591 antibody to PSMA-expressing tumors: optimization of imaging and therapy based on non-linear compartmental modeling. *EJNMMI Res.* 2016;6:7.

18. Wagner C, Zhao P, Pan Y, et al. Application of physiologically based pharmacokinetic (PBPK) modeling to support dose selection: report of an FDA public workshop on PBPK. *CPT Pharmacometrics Syst Pharmacol.* 2015;4:226-230.

19. Yao JC, Phan AT, Hess K, et al. Perfusion computed tomography as functional biomarker in randomized run-in study of bevacizumab and everolimus in well-differentiated neuroendocrine tumors. *Pancreas.* 2015;44:190-197.

20. Guyennon A, Mihaila M, Palma J, Lombard-Bohas C, Chayvialle JA, Pilleul F. Perfusion characterization of liver metastases from endocrine tumors: Computed tomography perfusion. *World J Radiol.* 2010;2:449-454.

21. Kimura H, Takeuchi H, Koshimoto Y, et al. Perfusion imaging of meningioma by using continuous arterial spin-labeling: comparison with dynamic susceptibility-weighted contrast-enhanced MR images and histopathologic features. *AJNR Am J Neuroradiol.* 2006;27:85-93.

22. Reidy-Lagunes D, Pandit-Taskar N, O'Donoghue JA, et al. Phase I trial of well-differentiated neuroendocrine tumors (NETs) with radiolabeled somatostatin antagonist (177)Lu-satoreotide tetraxetan. *Clin Cancer Res.* 2019;25:6939-6947.

23. Begum NJ, Glatting G, Wester H-J, Eiber M, Beer AJ, Kletting P. The effect of ligand amount, affinity and internalization on PSMA-targeted imaging and therapy: A simulation study using a PBPK model. *Sci Rep.* 2019;9:20041.

Figure legends

FIGURE 1.

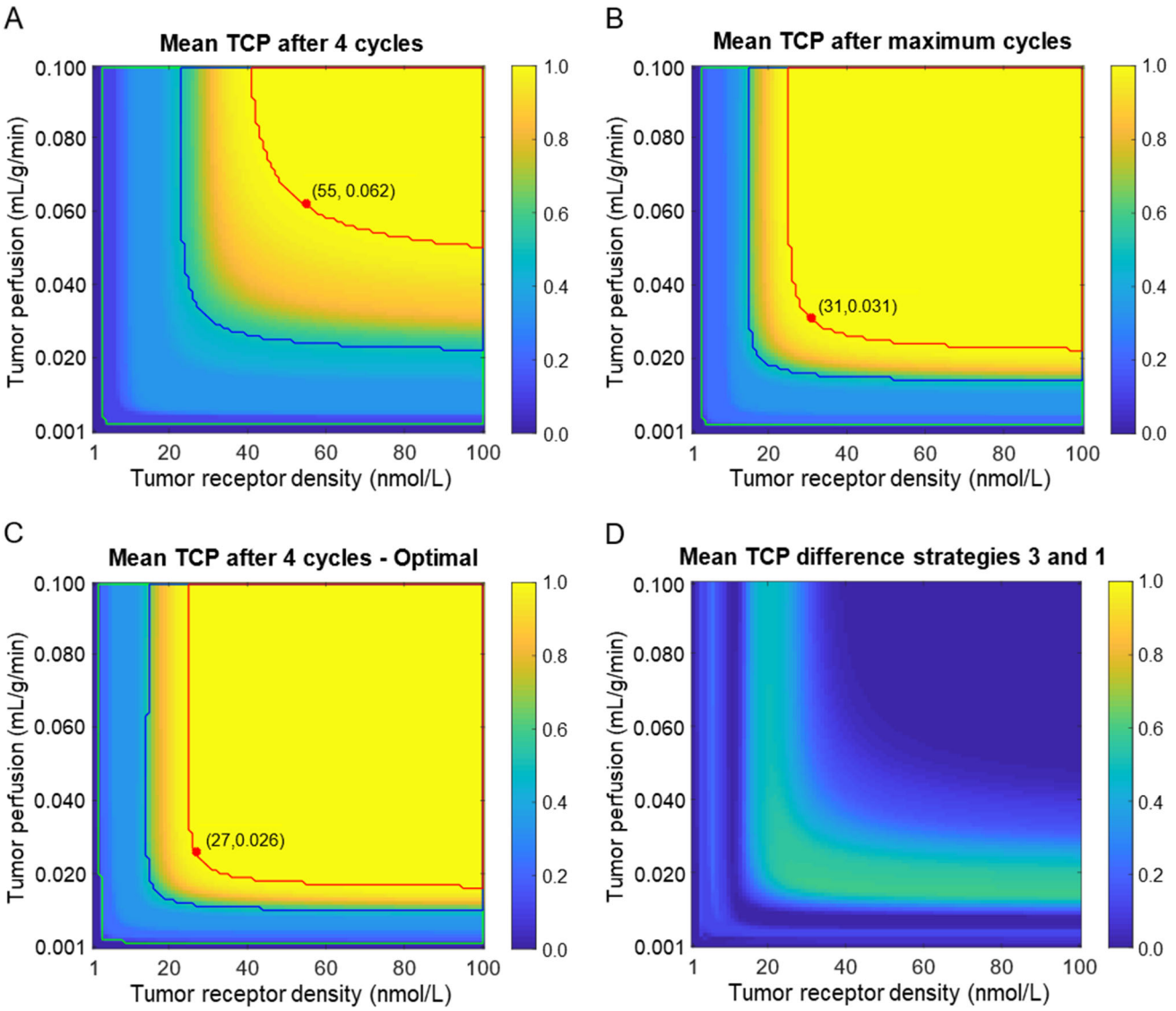

Figure 1: Mean tumor control probability (TCP) of all virtual patients is shown for different combinations of tumor perfusion and receptor density for different therapy strategies. In panel A, a standard treatment (strategy 1) was simulated, in panel B the number of cycles was optimized (strategy 2), and in panel C the ligand amount and the activity were optimized (strategy 3). The green, blue and red iso-TCP lines represent TCP values of 1%, 50% and 99%, respectively. The red stars show the combination of tumor perfusion and receptor density yielding TCP ≥99% with the smallest standardized Euclidean distance to the origin (0 nmol/L, 0 mL/g/min). Panel D depicts the mean TCP difference between strategy 3 and strategy 1.

FIGURE 2.

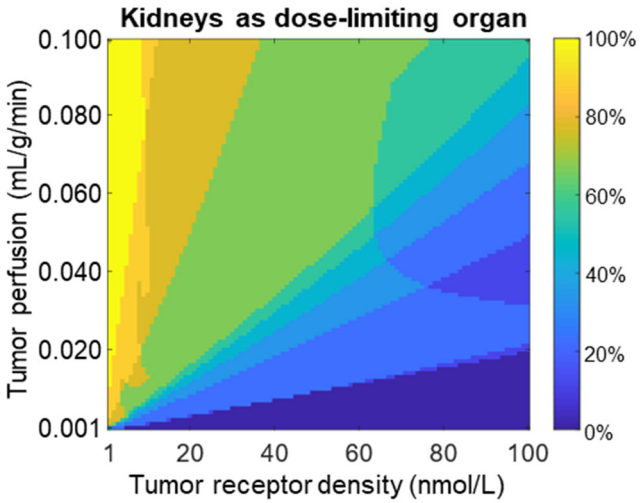

Figure 2 Fraction of virtual patients for which the kidneys are dose-limiting with strategy 3 for each combination of tumor perfusion and receptor density. 100% reflects that for these combinations the kidneys were dose-limiting in all patients. The complementary graph (Figure 2 subtracted from 100%) indicates the fraction of virtual patients for which the red marrow is dose-limiting for strategy 3.

FIGURE 3.

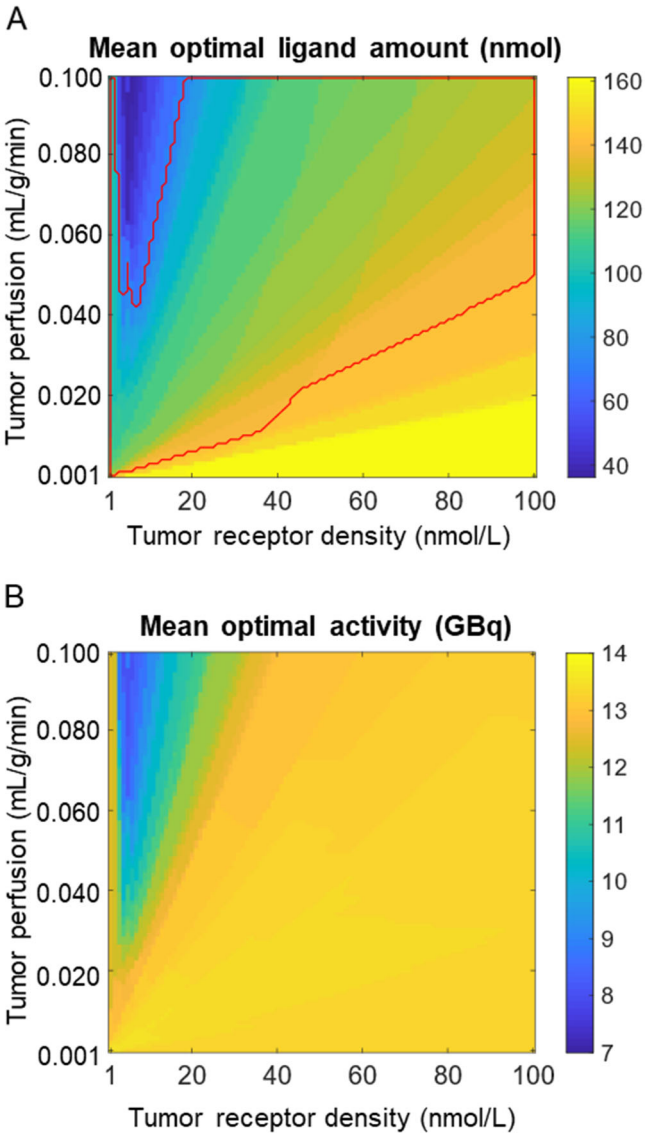

Figure 3 Mean optimal amounts (A) and activities (B) for one cycle for each combination of tumor perfusion and receptor density applying strategy 3. For the optimal amount (A), the red line contours the mean optimal amounts between 70 nmol (~ 100 µg) and 139 nmol (~200 µg) which is the consensual range of ligand amounts suggested by the EANM guidelines for therapy with peptides labeled with ^{177}Lu (*16*). The average optimal activity (B) was higher than the suggested maximum activity (7.4 GBq) for ^{177}Lu-DOTATATE treatment by the EANM guidelines for all the explored combinations (*16*).

Tables

TABLE 1: Investigated treatment strategies as determined by the number of cycles, the used ligand amount and activity and the OAR boundary conditions.

Strategy	Number of cycles	Ligand amount	Activity	Boundary condition OAR
1	4	105 nmol	7.4 GBq	None*
2	Maximized†	105 nmol	7.4 GBq	kidney $BED_{max} \leq 40$ $Gy_{2.5}$ and red marrow $BED_{max} \leq 2$ Gy_{15}
3	4	Optimal$	Optimal$	kidney $BED_{max} \leq 40$ $Gy_{2.5}$ and red marrow $BED_{max} \leq 2$ Gy_{15}

* not reached for all patients

†Maximized considering OAR BED_{max}

$ Maximal activity to be administered is calculated for amounts of 25, 50, 75, 100, 125, 150, 175, 200, 250, 350 and 500 nmol. Combination of amount and maximal activity resulting in highest TCP is selected.

TABLE 2: Individual minimal tumor perfusion and receptor density for each virtual patient and evaluated strategy to achieve a TCP >99%.

Virtual patient	Strategy 1		Strategy 2		Strategy 3		Actual values	
	$f_{tu,min}$* mL/g/min	$[R]_{tu,min}$† nmoL/L	$f_{tu,min}$* mL/g/min	$[R]_{tu,min}$† nmol/L	$f_{tu,min}$* mL/g/min	$[R]_{tu,min}$† nmol/L	$f_{tu}$$ mL/g/min	$[R]_{tu}$§ nmol/L
VP1	0.044	41	0.025	23	0.019	19	0.1	15
VP2	0.051	47	0.028	27	0.023	22	0.1	24
VP3	0.054	53	0.036	35	0.029	31	0,9	5
VP4	0.072	63	0.031	27	0.026	25	1	30
VP5	0.004	5	0.004	5	0.004	4	0,1	29
VP6	0.043	42	0.024	24	0.021	21	1	19
VP7	0.011	10	0.006	6	0.006	5	0.03	11
VP8	0.011	15	0.011	15	0.011	10	0.02	16
VP9	0.032	31	0.032	31	0.022	29	0.06	14
Mean	0.036	34.1	0.022	21.4	0.018	18.4	0.4	18
Std	0.023	20.2	0.012	10.6	0.009	10.0	0.4	8
Median	0.044	42	0.025	24	0.021	21	0.1	16
Min	0.004	5	0.004	5	0.004	4	0.02	5
Max	0.072	63	0.036	35	0.029	31	1	30

* $f_{tu,min}$ minimal tumor perfusion, † $[R]_{tu,min}$ minimal tumor receptor density $ f_{tu} fitted tumor perfusion and § $[R]_{tu}$ fitted tumor receptor density

TABLE 3: Influence of varying tumor and normal tissue parameters on the minimal tumor perfusion and receptor density in the population median virtual patient

Parameter	Parameter values	Strategy 1		Strategy 2		Strategy 3	
		$f_{tu,min}$ * mL/g/min	$[R]_{tu,min}$ † nmol/L	$f_{tu,min}$ * mL/g/min	$[R]_{tu,min}$ † nmol/L	$f_{tu,min}$ * mL/g/min	$[R]_{tu,min}$ † nmol/L
Release rates [min^{-1}]	10^{-3}	0.100$	100$	0.065	62	0.055	54
	10^{-4}	0.032	31	0.018	18	0.016	16
	10^{-5}	0.017	16	0.010	9	0.009	8
	10^{-6}	0.015	15	0.009	8	0.008	7
Tumor volume [mL]	0.1	0.035	35	0.020	20	0.018	17
	1	0.041	41	0.024	23	0.021	20
	10	0.047	47	0.027	26	0.024	23
	100	0.049	49	0.028	27	0.024	24
GFR [mL/min]	30	0.023	24	0.029	33	0.021	28
	60	0.036	36	0.029	29	0.024	24
	90	0.048	48	0.027	27	0.024	23
	120	0.06	59	0.026	26	0.024	23
Kidney receptor density [nmol/L]	2.5	0.047	46	0.017	16	0.018	15
	5	0.047	47	0.021	20	0.021	20
	7.5	0.048	48	0.032	31	0.025	25
	10	0.049	48	0.049	48	0.027	33

* $f_{tu,min}$ minimal tumor perfusion, † $[R]_{tu,min}$ minimal tumor receptor density

$ Did not reach 99% TCP within the simulated ranges for tumor perfusion and receptor density.

Supplemental A: Equations, parameters and compartments

PBPK Model equations

The following equations describe the transport of labeled (indexed with *) and unlabeled peptide via blood flow, extravasation, binding, internalization, degradation and release, excretion and radioactive decay. The peptide was injected as a 51±8 min infusion for pre-therapeutic measurements. The variables are defined in Table A.

Bound and internalized peptide:

Liver, spleen, tumor, kidney, red marrow (RM), gastrointestinal track (GI), muscle, prostate/uterus, adrenals and rest.

Constraint for total sst2 receptors $R_{0,i}$

$$R_{0,i} = R_i + RP_i + RP_i^* \tag{1}$$

Internalized peptide

$$\begin{aligned} \frac{d}{dt} P_{\text{intern i}} &= \lambda_{\text{int},i} \cdot RP_i - \lambda_{release,i} \cdot P_{\text{intern } i} + \lambda_{phy} \cdot P^*_{\text{intern } i} \\ \frac{d}{dt} P^*_{\text{intern } i} &= \lambda_{\text{int},i} \cdot RP^*_{\ i} - \lambda_{release,i} \cdot P^*_{\text{intern } i} - \lambda_{phy} \cdot P^*_{\text{intern } i} \end{aligned} \tag{2}$$

Bound p

eptide on cell surface

$$\frac{d}{dt}RP_i = k_{on} \cdot P_{i,\text{int}} \cdot \frac{R_i}{V_{i,\text{int}}} - (k_{off} + \lambda_{\text{int},i}) \cdot RP_i + \lambda_{phy} \cdot RP_i^*$$
$$\frac{d}{dt}RP_i^* = k_{on} \cdot P_{i,\text{int}}^* \cdot \frac{R_i}{V_{i,\text{int}}} - (k_{off} + \lambda_{\text{int},i}) \cdot RP_i^* - \lambda_{phy} \cdot RP_i^* \quad (3)$$

Free peptide, vascular:

Transcapillary extravasation is described by the permeability surface area product (PS_i) and the vascular ($V_{i,v}$) and interstitial volumes ($V_{i,\text{int}}$) of the pertaining tissue. Convection from the vascular to the interstitial space is neglected as ^{177}Lu-DOTATATE represents a rather small molecule.

All tissues except kidneys and lungs

$$\frac{d}{dt}P_{i,v} = PS_i\left(\frac{P_{i,\text{int}}}{V_{i,\text{int}}} - \frac{P_{i,v}}{V_{i,v}}\right) + F_i\left(\frac{P_{ART}}{V_{ART}} - \frac{P_{i,v}}{V_{i,v}}\right) + \lambda_{phy} \cdot P_{i,v}^*$$
$$\frac{d}{dt}P_{i,v}^* = PS_i\left(\frac{P_{i,\text{int}}^*}{V_{i,\text{int}}} - \frac{P_{i,v}^*}{V_{i,v}}\right) + F_i\left(\frac{P_{ART}^*}{V_{ART}} - \frac{P_{i,v}^*}{V_{i,v}}\right) - \lambda_{phy} \cdot P_{i,v}^* \quad (4)$$

For brain PS = 0

Lungs

$$\frac{d}{dt}P_{LU,v} = PS_{LU}\left(\frac{P_{LU,\text{int}}}{V_{LU,\text{int}}} - \frac{P_{LU,v}}{V_{LU,v}}\right) + F\left(\frac{P_{VEN}}{V_{VEN}} - \frac{P_{LU,v}}{V_{LU,v}}\right) + \lambda_{phy} \cdot P_{LU,v}^*$$
$$\frac{d}{dt}P_{LU,v}^* = PS_{LU}\left(\frac{P_{LU,\text{int}}^*}{V_{LU,\text{int}}} - \frac{P_{LU,v}^*}{V_{LU,v}}\right) + F\left(\frac{P_{VEN}}{V_{VEN}} - \frac{P_{LU,v}^*}{V_{LU,v}}\right) - \lambda_{phy} \cdot P_{LU,v}^* \quad (5)$$

Kidneys

$$\frac{d}{dt}P_{K,v} = -\frac{P_{K,v}}{V_{K,v}}\cdot(F_{fil}+F_K)+\frac{F_K}{V_{ART}}\cdot P_{\mathrm{ART}}+\frac{P_{\mathrm{intra,K}}}{V_{\mathrm{intra,K}}}\cdot(F_{fil}-F_{ex})+\lambda_{phy}\cdot P^*_{K,v}$$
$$\frac{d}{dt}P^*_{K,v} = -\frac{P^*_{K,v}}{V_{K,v}}\cdot(F_{fil}+F_K)+\frac{F_K}{V_{ART}}\cdot P^*_{\mathrm{ART}}+\frac{P^*_{\mathrm{intra,K}}}{V_{\mathrm{intra,K}}}\cdot(F_{fil}-F_{ex})-\lambda_{phy}\cdot P^*_{K,v} \quad (6)$$

Veins

$$\frac{d}{dt}P_{\mathrm{VEN}} = -k_{\mathrm{Pr}}\cdot P_{\mathrm{VEN}}+\sum\frac{F_i}{V_i}P_{i,\mathrm{v}}-\frac{F_M}{V_M}P_{M,\mathrm{v}}-\frac{F_{GI}}{V_{GI}}P_{\mathrm{GI,v}}+\frac{F_M+F_{GI}}{V_L}P_{L,\mathrm{v}}+\lambda_{phy}\cdot P^*_{\mathrm{VEN}}$$
$$\frac{d}{dt}P^*_{VEN} = -k_{\mathrm{Pr}}\cdot P^*_{VEN}+\sum\frac{F_i}{V_i}P^*_{i,\mathrm{v}}-\frac{F_M}{V_M}P^*_{M,\mathrm{v}}-\frac{F_{GI}}{V_{GI}}P^*_{\mathrm{GI,v}}+\frac{F_M+F_{GI}}{V_L}P^*_{L,\mathrm{v}}-\lambda_{phy}\cdot P^*_{\mathrm{VEN}} \quad (7)$$

Arteries

$$\frac{d}{dt}P_{\mathrm{ART}} = -\sum\frac{F_i}{V_{ART}}\cdot P_{i,\mathrm{v}}+\frac{F}{V_{LU,v}}\cdot P_{\mathrm{LU,v}}+\lambda_{phy}\cdot P^*_{ART}$$
$$\frac{d}{dt}P^*_{ART} = -\sum\frac{F_i}{V_{ART}}\cdot P_{i,\mathrm{v}}+\frac{F}{V_{LU,v}}\cdot P_{\mathrm{LU,v}}-\lambda_{phy}\cdot P^*_{ART} \quad (8)$$

<u>Free peptide, interstitial spaces:</u>

Kidneys:

$$\frac{d}{dt}P_{K,\mathrm{int}} = -k_{on}\cdot P_{K,\mathrm{int}}\cdot\frac{R_K}{V_{K,\mathrm{int}}}+k_{off}\cdot RP_K+F_{fil}\left(\frac{P_{K,v}}{V_{K,v}}-\frac{P_{K,\mathrm{int}}}{V_{K,\mathrm{int}}}\right)+\lambda_{phy}\cdot P^*_{K,\mathrm{int}}$$
$$\frac{d}{dt}P^*_{K,\mathrm{int}} = -k_{on}\cdot P^*_{K,\mathrm{int}}\cdot\frac{R_K}{V_{K,\mathrm{int}}}+k_{off}\cdot RP^*_K+F_{fil}\left(\frac{P^*_{K,v}}{V_{K,v}}-\frac{P^*_{K,\mathrm{int}}}{V_{K,\mathrm{int}}}\right)-\lambda_{phy}\cdot P^*_{K,\mathrm{int}} \quad (9)$$

Skin, adipose tissue, heart, bone, lungs and brain (PS = 0):

$$\begin{aligned}\frac{d}{dt}P_{i,\text{int}} &= PS_i\left(\frac{P_{i,v}}{V_{i,v}}-\frac{P_{i,\text{int}}}{V_{i,\text{int}}}\right)+\lambda_{phy}\cdot P^*_{i,\text{int}}\\ \frac{d}{dt}P^*_{i,\text{int}} &= PS_i\left(\frac{P^*_{i,v}}{V_{i,v}}-\frac{P^*_{i,\text{int}}}{V_{i,\text{int}}}\right)-\lambda_{phy}\cdot P^*_{i,\text{int}}\end{aligned} \tag{10}$$

Liver, spleen, tumor, RM, GI, muscle, prostate/uterus, adrenals, rest:

$$\begin{aligned}\frac{d}{dt}P_{i,\text{int}} &= -k_{on}\cdot P_{i,\text{int}}\cdot\frac{R_i}{V_{i,\text{int}}}+k_{off}\cdot RP_i+PS_i\left(\frac{P_{i,v}}{V_{i,v}}-\frac{P_{i,\text{int}}}{V_{i,\text{int}}}\right)+\lambda_{phy}\cdot P^*_{i,\text{int}}\\ \frac{d}{dt}P^*_{i,\text{int}} &= -k_{on}\cdot P^*_{i,\text{int}}\cdot\frac{R_i}{V_{i,\text{int}}}+k_{off}\cdot RP_i{}^*+PS_i\left(\frac{P^*_{i,v}}{V_{i,v}}-\frac{P^*_{i,\text{int}}}{V_{i,\text{int}}}\right)-\lambda_{phy}\cdot P^*_{i,\text{int}}\end{aligned} \tag{11}$$

Further equations:

Peptide in kidney cells (unspecific)

$$\begin{aligned}\frac{d}{dt}P_{\text{intra,K}} &= \frac{P_{\text{int,K}}}{V_{\text{int},K}}\cdot(F_{fil}-F_{ex})-\frac{P_{\text{intra,K}}}{V_{\text{intra,K}}}\cdot(F_{fil}-F_{ex})+\lambda_{phy}\cdot P^*_{\text{intra,K}}\\ \frac{d}{dt}P^*_{\text{intra,K}} &= \frac{P^*_{\text{int,K}}}{V_{\text{int},K}}\cdot(F_{fil}-F_{ex})-\frac{P^*_{\text{intra,K}}}{V_{\text{intra,K}}}\cdot(F_{fil}-F_{ex})-\lambda_{phy}\cdot P^*_{\text{intra,K}}\end{aligned} \tag{12}$$

Bound to protein

$$\begin{aligned}\frac{d}{dt}PPR &= k_{PR}\cdot P_{VEN}+\lambda_{phy}\cdot PPR^*\\ \frac{d}{dt}PPR^* &= k_{PR}\cdot P^*_{VEN}-\lambda_{phy}\cdot PPR^*\end{aligned} \tag{13}$$

PBPK Model compartments

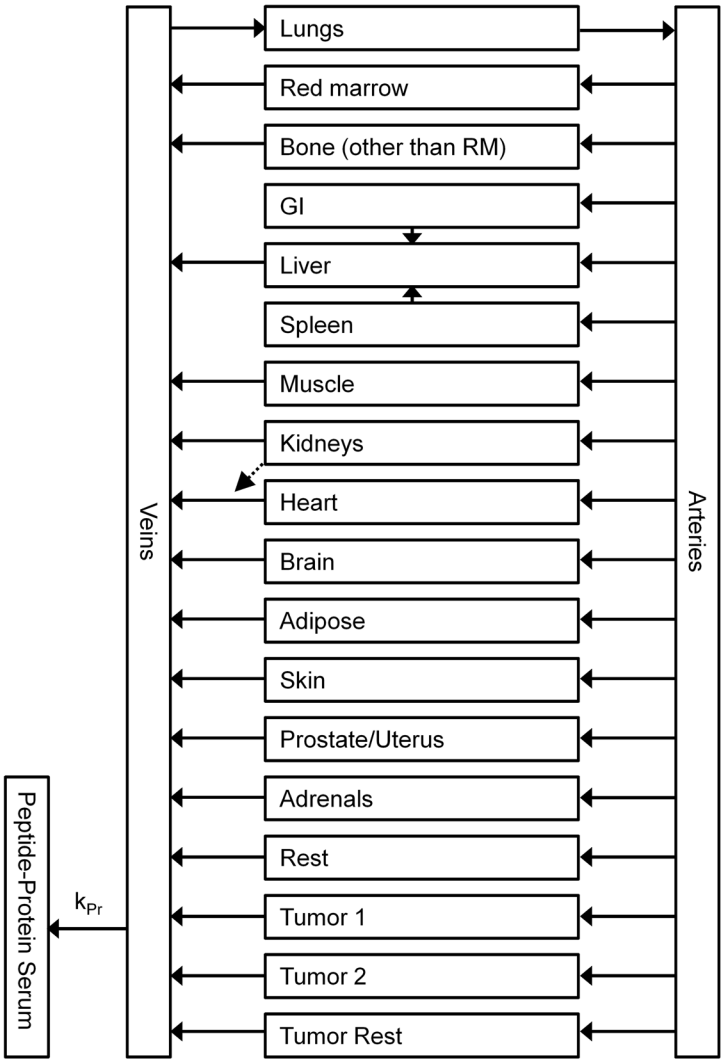

Figure 1: Main model structure: All organs are represented by a rectangular compartment and are connected via blood flow. Each organ within this model, except arteries, veins, brain and protein serum, is divided into sub-compartments. The substance is cleared via kidneys. The compartment "Peptide-Protein serum" contains peptide bound to serum protein. As the fraction of bound peptide to proteins compared to the total amount is small and to reduce the complexity, only the „veins" were connected to this compartment. The corresponding fraction for each specific organ was considered in the fitting process by assigning the data to the specific compartments.

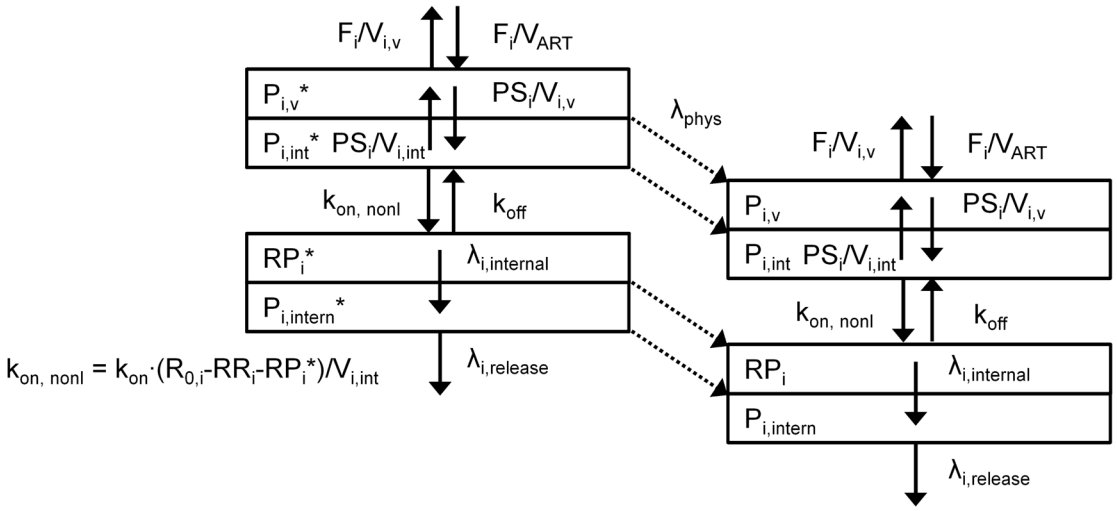

Figure 2a: Red marrow, GI, spleen, muscle, prostate (uterus), adrenals, rest and tumor: The entire model consists of two systems, one for labeled (with *) and one for unlabeled peptide. The systems are connected by the competition for free receptors ($k_{on,nonl} = k_{on} \cdot (R_{0,i}\text{-}RR_i\text{-}RP_i^*)/V_{i,int}$) and by the physical decay (λ_{phys}). All physiological parameters are assumed equal for the labeled and unlabeled substance. k_{off} is the dissociation rate, the transport of peptide via serum flow to organ is described by F_i/V_{ART} (where F_i is serum flow and V_{ART} is serum volume of the arteries). $F_i/V_{i,v}$ describes the transport of peptide via serum flow out of organ. $V_{i,v}$ is the serum volume of the respective organ. RP_i is sst2 specific bound peptide to the cell surface. $P_{i,v}$ and $P_{i,int}$ are free peptide of the vascular ($V_{i,v}$) and interstitial space ($V_{i,int}$), respectively. PS_i is the permeability surface area product. $\lambda_{i,internal}$ is the internalisation rate of bound peptide and $\lambda_{i,release}$ the release rate of ^{177}Lu (and degraded peptide) from the cell.

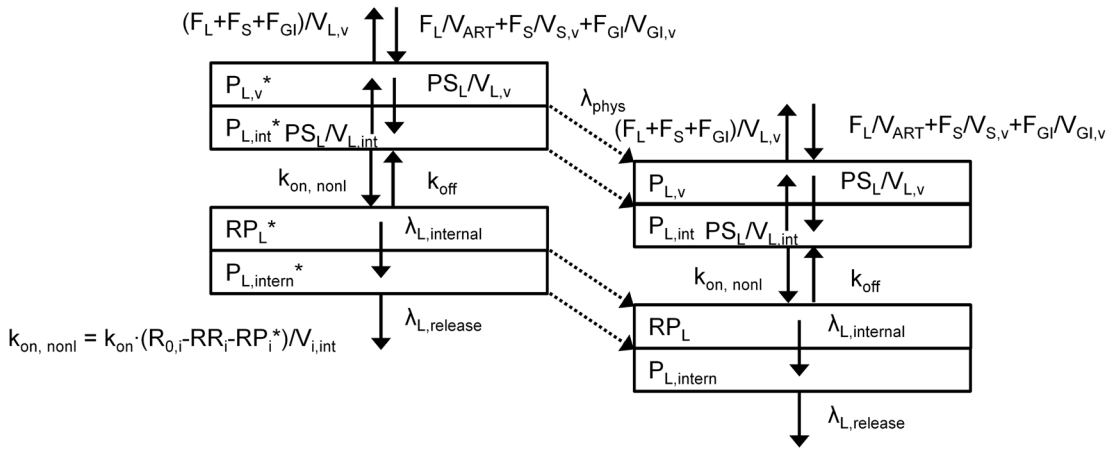

Figure 2b: Liver: For the liver, the model description of Figure 2a applies but the plasma flow is composed of liver arterial, GI and spleen flow.

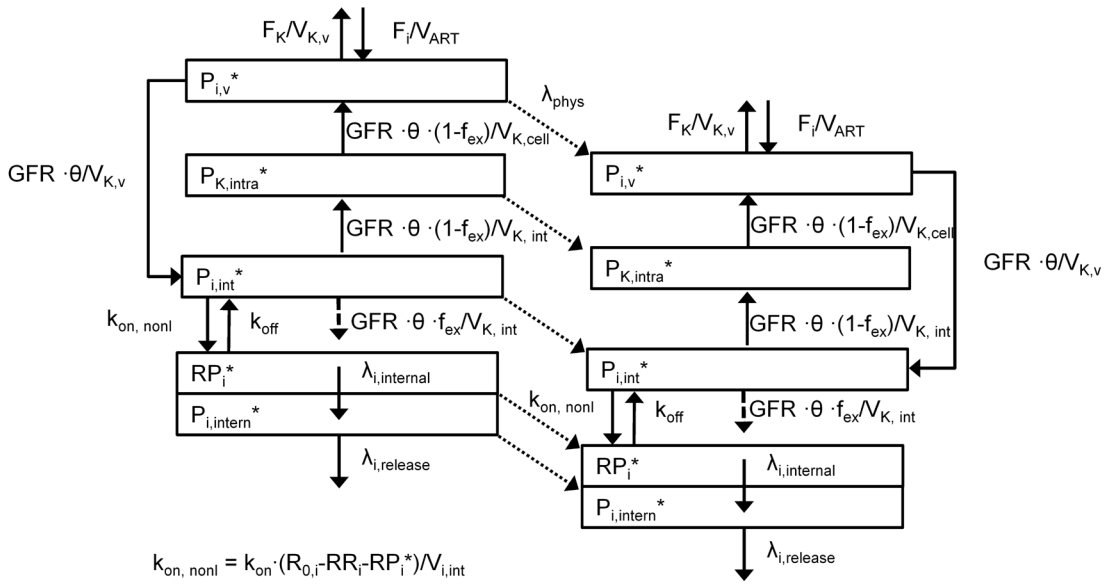

Figure 2c: Kidneys: The peptide is transported via serum flow to the vascular compartment and then filtrated into the interstitial part. Due to the administration of amino acids the largest fraction (f_{ex} = 0.98, Table A) of peptide is excreted. All unspecific uptake mechanisms are modelled with flow GFR ·θ ·(1-f_{ex}) in and out of kidney cells.

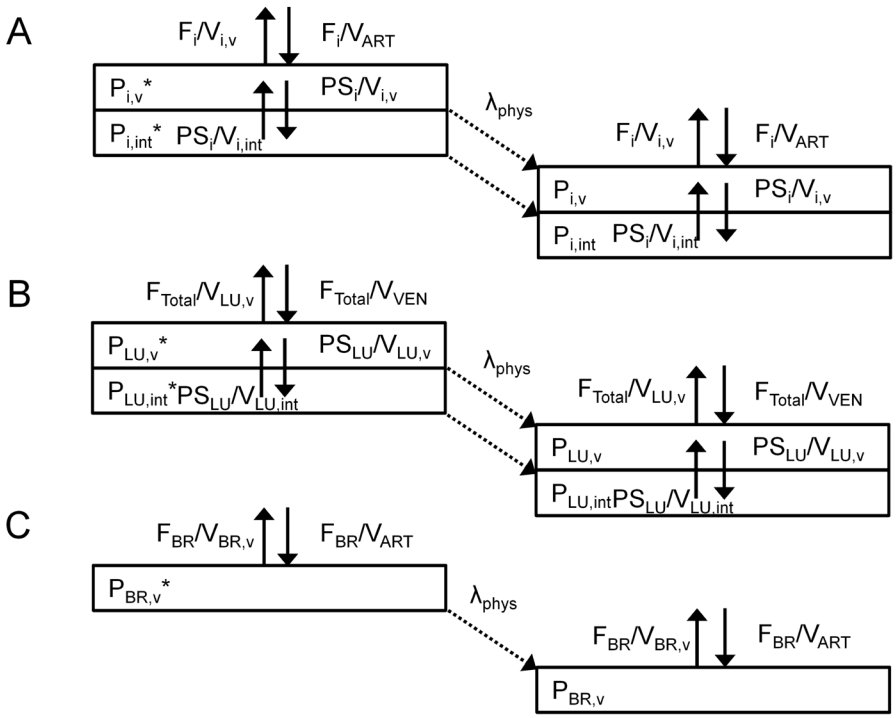

Figure 3: sst2 negative tissue and brain: For adipose, bone (other than red marrow), skin, heart (A) and lung (B), the model on the organ level simplifies to the transport of peptide via serum flow and transcapillary extravasation. For brain (C) the model reduces to serum flow.

TABLE 1 Parameter definition (1)

Variable		Value	Unit
k_{on}	association rate	k_{off} / K_D	$l \cdot nmol^{-1} \cdot min^{-1}$
k_{off}	dissociation rate	0.04	min^{-1}
K_D	dissociation constant	0.5	$nmol \cdot l^{-1}$
λ_{phy}	physical decay ^{177}Lu	$7.238 \cdot 10^{-5}$	min^{-1}
BW	body weight	individually measured	kg
H	hematocrit	individually measured	unity
F	flow total serum	$V_P \cdot 1.23/min^b$	$l \cdot min^{-1}$
V_P	volume of total body serum	male 2.8·(1- H)·BSA female 2.4·(1- H)·BSA	l
Tumor			
$V_{TU,total}$	total volume of tumor 1 and 2	measured	l
$V_{TU,\ int}$	interstitial space of tumor	$v_{tu,int} \cdot V_{Tu\ total}$	l
$V_{TU,\ v}$	vascular space of tumor	$v_{tu,v} \cdot V_{Tu\ total}$ (1-H)	l
$v_{TU,int}$	interstitial space fraction of total tumor	0.3 for NET 0.23 for meningioma	unity
$v_{TU,v}$	vascular fraction of total tumor	0.1 for NET 0.11 for meningioma	unity
F_{TU}	serum flow tumor	$f_{tu} \cdot (1\text{-}H) \cdot V_{total,Tu}$	$l \cdot min^{-1}$
f_{TU}	serum flow density tumor/perfusion	fitted/simulated	$ml \cdot min^{-1} \cdot g^{-1}$
PS_{TU}	permeability surface area product	$k_{TU} \cdot V_{Tu,\ total}$	$ml \cdot min^{-1}$
k_{TU}	permeability surface area product per unit mass (scaled for molecule size of DOTATATE)	0.2 NET metastasis 0.31 meningioma	$ml \cdot min^{-1} \cdot g^{-1}$
$[R_{TU,0}]$	sst2 receptor density tumour	fitted/simulated	$nmol \cdot l^{-1}$
$R_{TU,0}$	sst2 receptor number tumour	$[R_{TU,0}] \cdot V_{Tu,total}$	nmol
$\lambda_{TU,int}$		0.001	min^{-1}
$\lambda_{TU,release}$		fitted	min^{-1}
Measured organs			
$V_{L,total}$	volume total liver	individually measured	l
$V_{S,total}$	volume total spleen	individually measured	l
$V_{K,total}$	volume total kidney	individually measured	l
$V_{i,v}$	Vascular (serum) volume organ liver, spleen, kidney	$V_{i,total} \cdot v_{i,v}$	l
$V_{i,int}$	interstitial volume liver, spleen, kidneys	$V_{i,total} \cdot v_{i,int}$	l
$V_{K,\ intra}$	volume intracellular kidney	$(V_{K,total} - V_{K,int} - V_{K,v}) \cdot 2/3^c$	l
$v_{L,v}$	vascular (serum) fraction liver	0.085	unity
$v_{S,v}$	vascular (serum) fraction spleen	0.12	unity
$v_{K,v}$	vascular (serum) fraction kidneys	0.055	unity
$v_{L,int}$	interstitial fraction liver	0.2	unity
$v_{S,int}$	interstitial fraction spleen	0.2	unity
$v_{K,int}$	interstitial fraction kidney	0.15	unity
F_L	serum flow liver arterial	0.065·F	$l \cdot min^{-1}$
F_S	serum flow spleen	0.03·F	$l \cdot min^{-1}$
F_K	serum flow kidneys	0.19·F	$l \cdot min^{-1}$
φ	ratio of sieving coefficients	$\Theta_{DOTATATE}$ / $\theta_{Cr\text{-}51\text{-}EDTA}$	unity
F_{fil}	filtration	$GFR_{measured} \cdot \varphi^d$	$l \cdot min^{-1}$
F_{ex}	excretion	$F_{fil} \cdot f_{ex}$	$l \cdot min^{-1}$
f_{ex}	excretion/filtration	0.98	unity
k_L	permeability surface area product per unit mass for liver	$k_{MUS} \cdot 100$	$ml \cdot min^{-1} \cdot g^{-1}$
k_S	permeability surface area product per unit mass for spleen	k_L (due to similar capillary structure)	$ml \cdot min^{-1} \cdot g^{-1}$
$[R_{L,0}]$	receptor density liver	fitted	$nmol \cdot l^{-1}$

$[R_{S,0}]$	receptor density spleen	fitted	$nmol \cdot l^{-1}$
$[R_{K,0}]$	receptor density kidneys	fitted	$nmol \cdot l^{-1}$
$\lambda_{L,int}$	internalization rate sst2 liver	$\lambda_{K,int}$	min^{-1}
$\lambda_{S,int}$	internalization rate sst2 spleen	$\lambda_{K,int}$	min^{-1}
$\lambda_{K,int}$	internalization rate sst2 kidneys	$\Lambda_{TU,int} \cdot 1.7^{e}$	min^{-1}
$\lambda_{L,release}$	release rate liver	$\lambda_{NT,release}$	min^{-1}
$\lambda_{S,release}$	release rate spleen	$\lambda_{NT,release}$	min^{-1}
$\lambda_{K,release}$	release rate kidneys	$\lambda_{NT,release}$	min^{-1}
Other organs			
$V_{PRO,total}$ $V_{UT,total}$	volume total prostate volume total uterus	0.016·BW/71 0.080·BW/71	l
$V_{LU,total}$	volume total lungs	1·BW/71	l
$V_{AD,total}$	volume total adrenals	0.014·BW/71	l
$V_{MUS,total}$	volume total muscles	30.078·BW/71	l
$V_{GI,total}$	volume total GI + pancreas	(0.385+0.548+0.104+0.15)·BW/71	l
$V_{SKIN,total}$	volume total skin	3.408·BW/71	l
$V_{ADI,total}$	volume total adipose tissue	13.465·BW/71	l
$V_{RM,total}$	volume total red marrow	1.1·BW/71	l
$V_{BONE,total}$	volume total bone without red marrow	10.165·BW/71 - $V_{RM,total}$	l
$V_{HRT,total}$	volume total heart	0.341·BW/71	l
$V_{BR,total}$	volume total brain	1.45·BW/71	l
V_{BW}	volume of total body based on BW	1 ml ≙ 1 g	l
$V_{REST,total}$	volume of rest body i = all organs except tumor	$V_{BW} - \sum_i V_{i,total}$	l
$V_{PRO,v}$ $V_{UT,v}$	vascular fraction prostate/uterus	0.04 · (1-H) · $V_{PRO,total}$ 0.07 · (1-H) · $V_{UT,total}$	l
$V_{LU,v}$	vascular (serum) volume lungs	0.105 · V_P	l
$V_{AD,v}$	vascular (serum) volume adrenals	0.03 · (1-H) · $V_{AD,total}$	l
$V_{MUS,v}$	vascular (serum) volume muscles	0.14 · V_P	l
$V_{GI,v}$	vascular (serum) volume GI+ pancreas	0.076 · V_P	l
$V_{SKIN,v}$	vascular(serum) volume skin	0.03 · V_P	l
$V_{ADI,v}$	vascular(serum) volume adipose tissue	0.05 · V_P	l
$V_{RM,v}$	vascular(serum) volume red marrow	0.04 · V_P	l
$V_{BONE,v}$	vascular volume bone without red marrow	0.07 · V_P - V_{RM}	l
$V_{HRT,v}$	vascular (serum) volume heart	0.01 · V_P	l
$V_{BR,v}$	vascular(serum) volume brain	0.012 · V_P	l
$V_{REST,v}$	serum volume rest i = all organs except tumor	$V_P - \sum_i V_{i,v}$	l
V_{ART}	arterial serum plus ½ serum content of heart	0.06 · V_P + 0.045 · V_P	l
V_{VENES}	venous serum plus ½ serum content of heart	0.18 · V_P + 0.045 · V_P	l
$V_{PRO,int}$ $V_{UT,int}$	interstitial volume prostate/uterus	0.25 · $V_{PRO,total}$ 0.5 · $V_{UT,total}$	l
$V_{LU,int}$	interstitial volume lungs	$V_{LU,v} \cdot \alpha_{LU}$	l
$V_{AD,int}$	interstitial volume adrenals (the value for salivary gland is used)	0.24 · $V_{AD,total}$	l
$V_{MUS,int}$	interstitial volume muscles	$V_{MUS,v} \cdot \alpha_{MUS}$	l
$V_{GI,int}$	interstitial volume GI+ pancreas	$V_{GI,v} \cdot \alpha_{GI}$	l
$V_{SKIN,int}$	interstitial volume skin	$V_{SKIN,v} \cdot \alpha_{SKIN}$	l
$V_{ADI,int}$	interstitial volume adipose tissue	$V_{ADI,v} \cdot \alpha_{ADI}$	l
$V_{RM,int}$	interstitial volume red marrow	$V_{RM,v} \cdot \alpha_{RM}$	l
$V_{BONE,int}$	interstitial volume bone without red marrow	$V_{BONE,v} \cdot \alpha_{BONE}$	l

$V_{HRT,int}$	interstitial volume heart	$V_{HRT,v} \cdot \alpha_{HRT}$	l
$V_{REST,int}$	volume of rest body	$V_{REST,v} \cdot \alpha_{REST}$	l
α_{MUS}	ratio of interstitial to vascular volume average man	$V_{MUS,int}/V_{MUS,v} = 5.9$	unity
α_{GI}	ratio of interstitial to vascular volume average man	$V_{GI,int}/ V_{GI,v} = 8.8$	unity
α_{SKIN}	ratio of interstitial to vascular volume average man	$V_{SKIN,int}/ V_{SKIN,v} = 8.9$	unity
α_{ADI}	ratio of interstitial to vascular volume average man	$V_{ADI,int}/ V_{ADI,v} = 15.5$	unity
α_{RM}	ratio of interstitial to vascular volume average man	$V_{RM,int}/ V_{RM,v} = 3.7$	unity
α_{HRT}	ratio of interstitial to vascular volume average man	$V_{HRT,int}/ V_{HRT,v} = 3.7$	unity
α_{LU}	ratio of interstitial to vascular volume average man	$V_{LU,int}/ V_{LU,v} = 5.5$	unity
α_{BONE}	ratio of interstitial to vascular volume average man	$V_{BONE,int}/ V_{BONE,v} = 9.3$	unity
α_{REST}	ratio of interstitial to vascular volume average man	$V_{REST,int}/ V_{REST,v} = 3.7$	unity
f_{PRO}		0.18	$ml \cdot min^{-1} \cdot g^{-1}$
f_{UT}		1	$ml \cdot min^{-1} \cdot g^{-1}$
f_{AD}		6	$ml \cdot min^{-1} \cdot g^{-1}$
F_{PRO} F_{UT}	Total serum flow to prostate/uterus	$f_{PRO} \cdot (1\text{-}H) \cdot V_{PRO,total}$ $f_{UT} \cdot (1\text{-}H) \cdot V_{UT,total}$	$ml \cdot min^{-1}$
F_{LU}	Total serum flow lungs	F	$ml \cdot min^{-1}$
F_{AD}	Total serum flow to adrenals	$f_{AD} \cdot (1\text{-}H) \cdot V_{AD,total}$	$ml \cdot min^{-1}$
F_{MUS}	Total serum flow to muscle	$0.17 \cdot F$	$ml \cdot min^{-1}$
F_{GI}	Total serum flow to GI+ pancreas	$0.16 \cdot F$	$ml \cdot min^{-1}$
F_{SKIN}	Total serum flow to skin	$0.05 \cdot F$	$ml \cdot min^{-1}$
F_{ADI}	Total serum flow to adipose	$0.05 \cdot F$	$ml \cdot min^{-1}$
F_{RM}	Total serum flow to red marrow (RM)	$0.03 \cdot F$	$ml \cdot min^{-1}$
F_{BONE}	Total serum flow to bone (without RM)	$0.05 \cdot F$	$ml \cdot min^{-1}$
F_{HRT}	Total serum flow to heart	$0.04 \cdot F$	$ml \cdot min^{-1}$
F_{BR}	Total serum flow to brain	$0.12 \cdot F$	$ml \cdot min^{-1}$
F_{REST}	i = all organs except tumor	$F - \sum_i F_i$	$ml \cdot min^{-1}$
F_{TOTAL}		$F + F_{TU,1} + F_{TU,2} + F_{TU,REST}$	$ml \cdot min^{-1}$
PS_i	permeability surface area product	$k_i \cdot V_{i\ total}$	$ml \cdot min^{-1}$
k_{PRO} k_{UT}	permeability surface area product per unit mass (scaled for molecule size of DOTATATE) for prostate/uterus	0.1 0.2	$ml \cdot min^{-1} \cdot g^{-1}$
k_{LU}	permeability surface area product per unit mass for lungs	$k_{MUS} \cdot 100$	$ml \cdot min^{-1} \cdot g^{-1}$
k_{AD}	permeability surface area product per unit mass for adrenals	$k_{MUS} \cdot 100$(assumed to be very high as for salivary glands)	$ml \cdot min^{-1} \cdot g^{-1}$
k_{MUS}	permeability surface area product per unit mass for muscle	0.02	$ml \cdot min^{-1} \cdot g^{-1}$
k_{GI}	permeability surface area product per unit mass for GI and pancreas	0.02 (assumed to similar to muscle)	$ml \cdot min^{-1} \cdot g^{-1}$
k_{SKIN}	permeability surface area product per unit mass for skin	0.02 (assumed to similar to muscle)	$ml \cdot min^{-1} \cdot g^{-1}$

k_{ADI}	permeability surface area product per unit mass for adipose	0.02 (assumed to similar to muscle)	$ml \cdot min^{-1} \cdot g^{-1}$
k_{RM}	permeability surface area product per unit mass for red marrow	k_L(assumed to similar to liver)	$ml \cdot min^{-1} \cdot g^{-1}$
k_{HRT}	permeability surface area product per unit mass for heart	0.02 (assumed to similar to muscle)	$ml \cdot min^{-1} \cdot g^{-1}$
k_{BONE}	permeability surface area product per unit mass for bone	0.02 (assumed to similar to muscle)	$ml \cdot min^{-1} \cdot g^{-1}$
k_{REST}	permeability surface area product per unit mass for rest	0.02 (assumed to similar to muscle)	$ml \cdot min^{-1} \cdot g^{-1}$
$[R_{PRO,0}]$ $[R_{UT,0}]$	receptor density prostate based on sst2 density ratios calculated from (21)	$[R_{K,0}] \cdot 0.26$ $[R_{K,0}] \cdot 0.092$	$nmol \cdot l^{-1}$
$[R_{AD,0}]$	receptor density adrenals based on sst2 density ratios calculated from (21)	$[R_{K,0}] \cdot 1.65$	$nmol \cdot l^{-1}$
$[R_{MUS,0}]$	receptor density muscle based on sst2 density ratios calculated from (21)	$[R_{K,0}] \cdot 0.0056$	$nmol \cdot l^{-1}$
$[R_{GI,0}]$	receptor density GI + pancreas based on sst2 density ratios calculated from (21)	$[R_{K,0}] \cdot 0.16$	$nmol \cdot l^{-1}$
$[R_{RM,0}]$	receptor density RM based on sst2 density ratios calculated from (21)	$[R_{K,0}] \cdot 0.028$	$nmol \cdot l^{-1}$
$[R_{REST,0}]$	receptor density rest based on sst2 density ratios calculated from (21)	fitted	$nmol \cdot l^{-1}$
$\lambda_{NT,int}$	internalization rate for sst2 normal tissue	$\lambda_{K,int}$	min^{-1}
$\lambda_{NT,release}$	degradation and release from sst2 cells normal tissue	fitted	min^{-1}
R	receptors free		nmol
$R_{i,0}$	receptors total number of organ i	$[R_{i,0}] \cdot V_{i,total}$	nmol
$[R_{i,0}]$	receptor density of organ i		$nmol \cdot l^{-1}$
RP_i	peptide bound		nmol
PPR	peptide bound to serum protein		nmol
k_{PR}	binding rate peptide to serum	fitted	min^{-1}
P_{intern}	peptide internalized		nmol
$P_{i,v}$	peptide free vascular		nmol
$P_{i,int}$	peptide free interstitial		nmol
$P_{K,intra}$	peptide interacellular kidneys		nmol

[a]In house Biacore measurements (23) of PSMA specific peptides yielded typical values of 0.04 1/min. Ferl et al report similar values [1].

[b]For the average normal adult (blood) F = 6500 ml/min and V = 5300 ml. Therefore, a factor of 1.23 was assigned to account for the changes in total serum flow due to volume changes.

[c]It is assumed that 2/3 of the total intracellular volume of the kidney is represented by the proximal tubular cells

[d] Scaling of GFR due to different molecular sizes

[e] The mean value of the kidney to tumor ratio for the actually measured internalization rates was calculated. This average value of 1.7 was used as the ratio of kidney to the tumor internalization rate. (1)

Individual parameters of patients

The individualized PBPK model is defined as virtual patient. The parameters were fitted to time activity data as described in detail in Kletting et. al 2016 (1).

TABLE 2 Fitted parameters from Kletting et. al 2016 (1)

Patient	$[R_{K,0}]$	$[R_{S,0}]$	$[R_{L,0}]$	$[R_{REST,0}]$	$[R_{TU1,0}]$	$\lambda_{NT,release}$	$\lambda_{TU1,release}$	$V_{TURE,total,}$	f_{TU1}	k_{PR}
	[nmol/L]					$[min^{-1}\cdot 10^{-4}]$		[L]	$[ml\ min^{-1}\ g^{-1}]$	$[min^{-1}\cdot 10^{-4}]$
P1	6.5	8.7	1.4	0.5	15	0.7	1.1	-	0.10	4.7
P2	5.7	7.8	1.0	0.4	24	1.1	1.7	-	0.10	4.3
P3	6.2	17	0.9	0.4	5.0	0.5	3.0	-	0.90	4.0
P4	8.8	12	1.1	0.9	30	1.7	2.1	-	1.00	2.1
P5	7.1	13	1.2	0.5	29	2.1	0.0	0	0.10	24
P6	7.5	-	1.5	0.5	19	1.2	2.0	0.1	1.0	17
P7	2.8	3.9	1.1	0.5	11	1.2	0.0	0.0	0.03	10
P8	2.3	4.7	0.6	0.5	16	0.6	0.0	0.2	0.02	10
P9	8.7	18	2.1	0.5	14	1.4	2.1	1.2	0.06	17
Mean	6.2	10.6	1.2	0.5	18.1	1.2	1.3	0.2	0.37	10.3
SD	2.1	4.6	0.4	0.1	7.8	0.5	1.0	0.4	0.42	6.7

TABLE 3 Patient characteristics from Kletting et. al 2016 (1)

Patient	Disease*	Sex	Age	BSA† [m^2]	GFR‡ [l/min]	Measured volumes [ml]			
						Spleen	Liver	Kidneys	Tumor 1
P1	men	m	31	1.94	0.11	198	1811	193	87
P2	men	m	31	1.99	0.12	178	1824	185	116
P3	men	f	56	1.94	0.090	110	1500	125	2
P4	men	m	70	2.05	0.13	243	1896	206	3
P5	net	m	76	1.98	0.032	320	4876	147	2520§
P6	net	f	33	1.81	0.092	-‖	1897	156	4
P7	net	m	73	1.86	0.059	146	1804	157	111
P8	net	f	83	1.57	0.028	128	1610	233	13
P9	net	m	78	1.81	0.050	161	1900	156	3
Mean			52	1.89	0.11	180	2023	175	40
SD			22	0.12	0.12	61	910	29	44

* men = meningioma and net = neuroendocrine tumors † Body surface area ‡Measured glomerular filtration rate (GFR) using ^{51}Cr-EDTA §$V_{TU,total} = V_{L,total} - V_{L,total\ average}$ ‖splenectomy

References

1 .Kletting P, Kull T, Maaß C, et al. Optimized Peptide Amount and Activity for 90Y-Labeled DOTATATE Therapy. J Nucl Med. 2016;57:503-508.

Supplemental B: Absorbed Dose, BED and TCP

1. Absorbed dose calculations

Absorbed doses were calculated as follows:

$$D_{rT}(T) = Ao \cdot \sum_{rS=1}^{N} \tilde{a}_{rS}(T) \cdot S_{(rT \leftarrow rS)} \quad \text{(B1)}$$

where $D_{rT}(T)$ is the absorbed dose in a target region at time T, T is the radiation exposure time, Ao is the injected activity, rS the source region, N is the number of considered source regions, $\tilde{a}_{rS}(T)$ is the time-integrated activity coefficient for a source region at time T, and $S_{(rT \leftarrow rS)}$ is the dose factor (S value) from a source region (rS) to a target region (rT). $\tilde{a}_{rS}(T)$ values were calculated by integrating the normalized (by Ao) time activity curves (TACs) of the source regions from time 0 to time T. (*1*)

The following organs were considered as source regions (i.e. source organs): kidneys, liver, spleen, bone, muscle, red marrow, brain, heart, lungs, gastrointestinal track, adrenal glands and remainder of body. The kidneys and the red marrow were considered as target regions (i.e. target organs) for dose calculations.(*1*)

Due to the short mean penetration range of ^{177}Lu, only self-irradiation (i.e. $S_{(rT \leftarrow rS)} = 0$ for $rT \neq rS$ in Eq. (B1)) was considered in the absorbed dose calculations for the kidneys. As the red marrow (RM) is a distributed organ with high radiosensitivity, both self- and cross-irradiation were considered for the RM dose calculations.

The dose factors for ^{177}Lu were extracted from OLINDA/EXM v1.0 and individually scaled based on the target organ mass. The scaling factor (k_{rT}) for the dose factors was defined as:

$$k_{rT} = \frac{m_{rT\_patient}}{m_{rT\_phantom}} \quad \text{(B2)}$$

where $m_{rT\_patient}$ is the target organ mass in the patient and $m_{rT\_phantom}$ is the target organ mass used in OLINDA/EXM v1.0. Dose factors for the RM were scaled using the ratio between the patient body mass and the average body mass in OLINDA/EXM v1.0. Kidney volumes were individually measured and converted into kidney masses assuming a density of 1 g/ml. The dose factors for ^{177}Lu retrieved from OLINDA/EXM are presented in Table 1.

Table **1**. Dose factors for ^{177}Lu from OLINDA/EXM.

Parameter	**Value**	**Unit**
$S_{K\leftarrow K}$	4.82×10^{-6}	$\mathrm{Gy \cdot min^{-1} \cdot MBq^{-1}}$
$S_{RM\leftarrow RM}$	7.14×10^{-7}	$\mathrm{Gy \cdot min^{-1} \cdot MBq^{-1}}$
$S_{RM\leftarrow REM}$	4.83×10^{-9}	$\mathrm{Gy \cdot min^{-1} \cdot MBq^{-1}}$
$S_{RM\leftarrow AD}$	4.11×10^{-9}	$\mathrm{Gy \cdot min^{-1} \cdot MBq^{-1}}$
$S_{RM\leftarrow L}$	1.39×10^{-9}	$\mathrm{Gy \cdot min^{-1} \cdot MBq^{-1}}$
$S_{RM\leftarrow S}$	1.40×10^{-9}	$\mathrm{Gy \cdot min^{-1} \cdot MBq^{-1}}$
$S_{RM\leftarrow GI}$[a]	2.92×10^{-9}	$\mathrm{Gy \cdot min^{-1} \cdot MBq^{-1}}$
$S_{RM\leftarrow MUS}$	1.52×10^{-9}	$\mathrm{Gy \cdot min^{-1} \cdot MBq^{-1}}$
$S_{RM\leftarrow LU}$	1.84×10^{-9}	$\mathrm{Gy \cdot min^{-1} \cdot MBq^{-1}}$
$S_{RM\leftarrow K}$	2.84×10^{-9}	$\mathrm{Gy \cdot min^{-1} \cdot MBq^{-1}}$
$S_{RM\leftarrow BR}$	1.65×10^{-9}	$\mathrm{Gy \cdot min^{-1} \cdot MBq^{-1}}$
$S_{RM\leftarrow HRT}$	1.82×10^{-9}	$\mathrm{Gy \cdot min^{-1} \cdot MBq^{-1}}$
$S_{RM\leftarrow B}$[b]	2.04×10^{-7}	$\mathrm{Gy \cdot min^{-1} \cdot MBq^{-1}}$

Subscripts: K = Kidney; RM = Red marrow; REM = Remainder of body; AD = Adrenal glands; L = Liver; S = Spleen; GI = Gastrointestinal track; MUS = Muscle; LU = Lungs; BR = Brain; HRT = Heart; B = Bone.

[a] Dose factor for the small intestine.

[b] Dose factor for trabecular bone.

Tumor dose factors for ^{177}Lu were determined by fitting a power function to published data(*2*), based on the tumor lesion mass (assuming a tumor density of 1 g/ml). The data used for this fitting are presented in Table 2.

Table **2**. Reported dose factors for ^{177}Lu for tumor lesions based on tumor mass.(*2*)

Tumor mass [g]	**Tumor dose factor [Gy·min^{-1}·MBq^{-1}]**
0.5	2.77×10^{-3}
1	1.40×10^{-3}
1.5	9.00×10^{-4}
2	7.02×10^{-4}
3	4.50×10^{-4}
4	3.52×10^{-4}
13	1.10×10^{-4}
17	8.30×10^{-5}
21	6.90×10^{-5}
29	4.80×10^{-5}
34	4.30×10^{-5}
52	2.67×10^{-5}
54	2.65×10^{-5}

The fitted function for the tumor dose factors for ^{177}Lu is shown in Eq. (B3).

$$S_{TU} = 1.407 \cdot 10^{-3} \cdot {m_{TU}}^{-1} - 3.724 \cdot 10^{-5} \cdot {m_{TU}}^{(-2/3)} + 1.403 \cdot 10^{-5} \cdot {m_{TU}}^{(-1/3)} \qquad \text{(B3)}$$

where S_{TU} is the dose factor for a tumor lesion [Gy·min^{-1}·MBq^{-1}] and m_{TU} is the mass of the tumor lesion [g]. The adjusted R^2 value of the fitting was 0.9998.

2. Biological effective dose calculations

Biological effective doses (BEDs) were calculated according to:

$$BED_i = D_i \cdot \left(1 + \frac{G_i}{a_i/\beta_i} \cdot D_i\right) \quad \text{(B4)}$$

where a_i and β_i are the linear and quadratic parameters of the linear-quadratic (LQ) model for each tissue (a represents lethal DNA damage while β represents 'multiple hit' cell death resulting from the interaction of damage from different radiation tracks) , D_i is the absorbed dose in each tissue, and G_i is the Lea-Catcheside factor for each tissue, which accounts for sublethal damage repair during the radiation exposure. α/β ratios of 2.5 Gy ,15 Gy and 10 Gy were assumed for the kidneys, the RM and tumor lesions, respectively. The Lea-Catcheside factor at a time T ($G_i(T)$) for each tissue is defined in Eq. (B5). (*1*)

$$G_i(T) = \frac{2}{{D_i}^2} \cdot \int_0^T \dot{D}_i(t) \cdot \left(\int_0^t \dot{D}_i(w) \cdot e^{-\mu_{rep\_i} \cdot (t-w)} \cdot dw\right) \cdot dt \quad \text{(B5)}$$

where T is the radiation exposure time, t and w are integration time variables, and D_i, $\dot{D}_i(t)$ and μ_{rep_i} are the absorbed dose, the dose rate at time t and the cell repair rate after irradiation for each tissue, respectively. A μ_{rep} values of ln(2)/2.8 h^{-1}, ln(2)/1.0 h^{-1} and ln(2)/1.5 h^{-1} were used for the kidneys(*3*), the RM and the tumor lesions, respectively (*1*). The dose rate for each target tissue $\dot{D}_i(t)$ is defined as:

$$\dot{D}_i(t) = Ao \cdot \sum_{k=1}^{N} a_k(t) \cdot S_{(i \leftarrow k)} \quad \text{(B6)}$$

where Ao is the injected activity, N is the number of considered source tissues, $a_k(t)$ is the fraction of administered activity in the source tissue k at time t, and $S_{(i\leftarrow k)}$ is the dose factor from the source tissue k to the target tissue i (Table 1 and Eq. (B3)). $a_k(t)$ is obtained from the pharmacokinetic simulations in Matlab/Simulink®.

3. Tumor control probability calculations

Tumor control probability (TCP) considering one tumor lesion for a single PRRT cycle is defined as:

$$TCP = e^{-n_0 \cdot SF} \quad \text{(B7)}$$

where n_0 is the initial number of tumor clonogenic cells and SF is the survival fraction for a single PRRT cycle. The number of initial clonogenic cells for each tumor lesion was determined from the measured tumor mass and using a clonogenic cell density of 1.12×10^5 cells/g. The tumor survival fraction (SF) depends on the tumor BED and is defined as:

$$SF = e^{-\alpha \cdot BED} \quad \text{(B8)}$$

where a is the linear parameter (representing lethal DNA damage) of the LQ model (a = 0.35 Gy^{-1} for all tumor lesions[7]) and BED is the biological effective dose for the tumor lesion.

Assuming that there is no or negligible tumor repopulation between cycles, that the number of tumor clonogenic cells is large, that cell survival is a rare occurrence, and that cell death is stochastically independent of other cells; the TCP for multiple PRRT cycles for a single lesion can be defined as:

$$TCP = e^{-n_0 \cdot \sum_{c=1}^{N_c} SF_c} \quad \text{(B9)}$$

where n_0 is the initial number of tumor clonogenic cells, N_c is the number of cycles, and SF_c is the survival fraction for each of the PRRT cycle. Additionally, if the same SF is assumed for all the cycles,

which implies that the tumor physiological and pharmacokinetic characteristics do not change throughout the cycles, the TCP for multiple PRRT cycles for a single lesion can be described as:

$$TCP = e^{-n_0 \cdot \left(SF_c{}^{Nc}\right)} \quad \text{(B10)}$$

Calculations to determine TCP for multiple tumor lesions and multiple PRRT cycles can be found in Jimenez et al.(1)

REFERENCES

1. Jiménez-Franco LD, Kletting P, Beer AJ, Glatting G. Treatment planning algorithm for peptide receptor radionuclide therapy considering multiple tumor lesions and organs at risk. *Med Phys.* 2018;45:3516-3523.

2. Stabin MG, Siegel JA. Physical models and dose factors for use in internal dose assessment. *Health Phys.* 2003;85:294-310.

3. Cremonesi M, Botta F, Di Dia A, et al. Dosimetry for treatment with radiolabelled somatostatin analogues. A review. *Q J Nucl Med Mol Imaging.* 2010;54:37-51.